Machine learning-based radiomics for preoperative prediction of microvascular invasion in hepatocellular carcinoma

L. Xiong, Y. Peng, Sh. Li, X. Tang, J. Zhou, L. Gong*

Department of Medical Imaging Center, The Second Affiliated Hospital of Nanchang University, No. 1 Minde Road, Nanchang, Jiangxi, 330006, China

► *Original article*

*Corresponding author:
Dr. Lianggeng Gong
E-mail: gong111999@126.com

ABSTRACT

Background: Background: To evaluate the diagnostic performance of different radiomics models for preoperatively predicting microvascular invasion (MVI) of hepatocellular carcinoma (HCC). **Materials and Methods**: A total of 124 patients who had histologically confirmed HCC (training dataset: n=86; validation dataset: n=38) were included. Clinical factors (CFs) were extracted from medical data. Radiomics features were derived from the unenhanced phase, artery phase (AP), portal venous phase and delay phase CT images. The least absolute shrinkage and selection operator (LASSO) method was chosen to select the radiomics feature. Twelve models were established using three modeling methods (logistic regression [LR], support vector machine [SVM], and Bayes) with the radiomics signature. Receiver operating characteristic (ROC) analysis was used to evaluate the diagnostic performance of the models. A radiomics signature that performs well was integrated with the clinical factors into a combined model. **Results**: AP radiomics signatures achieved the best efficiency than other radiomics models. The LR model with the AP radiomics signature as the input factor showed better performance than the SVM and Bayes models, with an area under the curve (AUC) of 0.848 in the validation datasets. When integrating the AP radiomics signatures and clinical factors, the combined model performed better and reached an AUC of 0.875 in the validation datasets. **Conclusions**: The radiomics model demonstrated excellent performance for preoperatively predicting MVI in patients with HCC, especially the combined model. Different modeling methods could influence the effects of the diagnostic performance.

INTRODUCTION

Hepatocellular carcinoma (HCC) ranks as the 6th most prevalent form of cancer worldwide [1]. It is the third most common cause of cancer death, and more than half happened in China [2-4]. Tumor relapse remains the leading cause of death after surgery, with a 5-year overall survival of approximately 10–20% [5-7].

Microvascular invasion (MVI) is a definite risk factor for the recurrence of HCC after curative surgical therapies [8], and is a better predictor of tumor recurrence and OS than the commonly used Milan criteria. Practical preoperative evaluation of MVI in HCC can assist clinicians choose appropriate treatment approach for patients. Differs from macrovascular invasion, which can be easily detected by computed tomography (CT) and magnetic resonance (MR) imaging, MVI is currently only diagnosable by histopathology. Therefore, the challenge is to identify MVI in patients before any definitive therapy such as hepatectomy and liver transplantation.

Previous studies have shown that traditional imaging characteristics, clinical indicators, pathology and gene expression factors are associated with MVI, for example, the D value based on IVIM may predict MVI in HCC [9-11]. The results may be affected by the observers' subjective consciousness and lack of highly reliable factors. There is a need to explore whether there is a better way to predict MVI in HCC.

With the rapid development of technology, radiomics performs high-throughput mining of acquired imaging features, which provides predictive or prognostic information [12, 13]. It has achieved success in predicting the type of tumors by developing appropriate models [14]. Bakr *et al.* [15] showed that radiomics analysis of CT imaging was promising to assess MVI preoperatively in HCC with a noninvasive manner. In addition, He *et al.* found that the radiomics-based predictive model achieved satisfactory preoperative prediction of MVI in HCC patients [16]. However, few studies have interpreted and analyzed the similarities and differences within the results obtained from different modeling methods with multiple phases and explored which modeling

algorithm is most suitable for research.

This study aimed to validate whether a radiomics model combined machine learning could be more beneficial for predicting MVI in HCC than a clinical model. Additionally, we compared and analyzed the impact of different modeling methods on the MVI diagnostic performance.

MATERIALS AND METHODS

Patients

Our retrospective study was granted by the institutional ethics review board (registration number: No. 130, registration date: December 1, 2016), and a waiver of the requirement to obtain written informed consent was approved. Between January 2017 and May 2020, 327 HCC patients with pathologically confirmed after surgical resection were identified from the medical records. The following inclusion criteria were considered: (1) HCC patients with pathologically confirmed MVI status, (2) patients who underwent preoperative contrast-enhanced CT within two weeks of surgery, (3) without prior history of intervention treatment, and (4) no extrahepatic or lymph node metastasis. The exclusion criteria were as follows: (1) lack of complete clinical, pathological, or imaging data, (2) recurrent or multiple tumors, (3) unsatisfactory image quality. A total of 124 patients (median age, 55 years; interquartile range, 47-62 years; 98 men) were remained (figure 1). After random allocation into two groups at a ratio of 7:3, the numbers of patients in the training and validation datasets were 86 and 38, respectively.
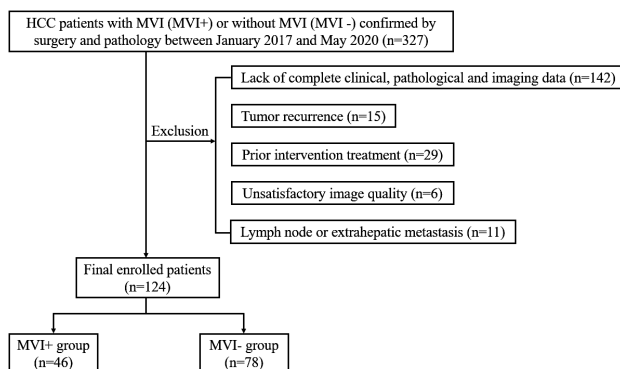

Figure 1. Process diagram of the study selection.

Routine preoperative laboratory examinations including sex, age, hepatitis B surface antigen (HBsAg) status, cirrhosis, maximum tumor diameter (MTD), postoperative pathological grading (well, moderate or poor), alpha-fetoprotein (AFP) level, alanine aminotransferase (ALT), aspartate aminotransferase (AST), platelet count (PLT) total bilirubin (TB), prothrombin time (PT), direct bilirubin (DB), and international normalized ratio (INR), were collected from our medical records system. Routine blood tests and liver function tests were conducted within 14 days prior to the surgery.

CT technology

All CT images were acquired using 128-row dual-source spiral CT scanners (Siemens Medical Systems, Erlangen, Germany). The routine plain scan was performed first, and then artery phase (AP) (25 s), portal venous phase (PVP) (50 s), and delay phase (DP) (110 s) were obtained after injection of 1.1 mL/kg of iopromide (Bayer HealthCare Pharmaceuticals Inc) into the cubital vein at a flow rate of 2.4 mL/s, followed by a 20 mL saline flush. The imaging parameters of CT were as follows: 120 kV tube voltage, 210 mAs, 0.5 s rotation time, 5 mm slice thickness, and a 5 mm interval, 250 × 250 mm field of view，256 × 256 matrices.

Development of radiomics technology

The radiomics workflow is divided into four procedures: tumor segmentation, radiomic feature extraction, predictive model building, and evaluation.
Tumor segmentation: The primary 3-dimensional volume of interests (VOIs) were manually delineated, slice-by-slice, by reader 1 (with five years of abdominal imaging experience) on each transverse section from the unenhanced, arterial, portal venous and delay phases using ITK-SNAP software (version 3.8.0, http://www.itksnap.org), and the final segmentation results were verified by reader 2 (with ten years of imaging experience).

Radiomic feature extraction and dimensionality reduction: All original images and VOIs were brought into the A.K. software (Artificial Intelligence Kit, GE Healthcare, China) for the texture process. A group of 396 radiomics features, including shape, size, intensity, and textural features, were extracted from the CT images in each phase.

One thousand five hundred eighty-four feature indices were preprocessed using mean or median substitution to replace some feature parameters with abnormal or missing values in each patient. Parameters were normalized into a feature matrix so that all features ranged between (0, 1). To quantify the reproducibility and stability of the descendent radiomics features, 40 randomly selected patients were segmented based on their tumors. We excluded features with intraclass correlation coefficient (ICC) less than 0.80. Finally, the least absolute shrinkage and selection operator (LASSO) method was applied, it is widely used to decrease the redundancy and irrelevance of radiomics features.

Clinical model and multiple machine learning model constructions: Radiomics model, clinical model, and combined model were established to predict the MVI status preoperatively.
Radiomics signatures were extracted from the

LASSO-selected features by R software (version 3.5.1, Boston, MA, USA). With the AP, PVP, DP, and unenhanced phase (UP) radiomics signatures as the input factors, 12 radiomics models were established using three modeling methods, involving logistic regression (LR), support vector machine (SVM) and Bayes. The model effectiveness of the three modeling methods and four phases were compared to select the optimal performance phase and modeling algorithm for establishing the clinical and combined models.

Clinical factors that were significantly associated with MVI were screened by stepwise variable selection. We applied the optimal performance modeling methods with the final selected clinical predictors for construction of the clinical model.

The combined model was constructed by integrating the radiomics signature in the best phase and the effective clinical predictors using the optimal performance modeling methods. The radiomics-based nomogram for predicting the risk of MVI was constructed with the LR model.

Model evaluation: ROC curves were plotted to quantify the efficiency of the models for identifying MVI. Sensitivity, specificity and accuracy were also obtained. Moreover, the DeLong test was performed to compare the area under the curves (AUCs) among the models. A calibration curve was plotted to intuitively assess the agreement between the predicted risk and actual risk of MVI, and a decision curve was implemented to evaluate the clinical usefulness of the combined model.

Statistical analysis

All statistical analyses were performed using SPSS (version 25, Chicago, IL, USA), R software, and IPMs (version 2.0.2, General Electric, USA). Categorical variables were compared using the Chi square test, and continuous variables were evaluated using the t-test or Mann–Whitney U test. Differences of $P<0.05$ were considered statistically significant.

RESULTS

Basic clinical characteristics

Based on the pathology reports, all patients were divided into the MVI present group (n=46) and the MVI absent group (n=78). Comparisons of the clinical characteristics between these two groups are summarized in table 1.

Stepwise variable selection showed that MTD (OR 1.981; 95% CI 1.132–3.466), PLT (OR 1.212; 95% CI 0.706–2.082), pathological grading (OR 1.986; 95% CI 0.995–3.964), and AFP (OR 1.383; 95% CI 0.835–2.292) were independent predictors of MVI. Both the training and validation groups showed statistically significant differences in MTD and HBsAg (P < 0.05). In the training dataset, pathological grading and AFP exhibited significant differences in the training group,

however, no differences were observed in the validation dataset (table 1).

Table 1. Comparisons of clinical characteristics in the training and validation datasets.

Characteristic	Training dataset (N=86)			Validation dataset (N=38)		
	MVI+ (N=32)	MVI- (N=54)	P value	MVI+ (N=14)	MVI- (N=24)	P value
Age (years), median	52	56	0.100	52	57	0.151
Gender						
Male	28	40	0.139	12	18	0.435
Female	4	14		2	6	
HBsAg						
Negative	2	14	0.023*	5	2	0.036*
Positive	30	40		9	22	
Cirrhosis						
Negative	13	22	0.992	6	7	0.391
Positive	19	32		8	17	
MTD (cm), median	7	3	0.004*	7	4	0.011*
Pathologic grade						
Well	0	8	0.005*	0	2	0.314
Moderately	24	43		12	21	
Poorly	8	3		2	1	
AFP, median	364.70	18.20	0.001*	40.45	13.55	0.574
ALT, median	36.49	32.30	0.288	29.91	32.97	0.304
AST, median	46.88	40.65	0.249	32.66	43.15	0.397
TB, median	16.65	16.42	0.411	16.06	15.49	0.380
DB, median	3.45	3.47	0.574	4.02	4.17	0.325
PLT, median	163.00	161.50	0.496	206.50	133.50	0.053
PT, median	12.30	12.00	0.260	12.55	11.85	0.150
INR, median	1.06	1.02	0.202	1.08	1.02	0.154

HBsAg hepatitis B surface antigen, *MTD* maximum tumor diameter, *AFP* alpha-fetoprotein, *ALT* alanine aminotransferase, *AST* aspartate aminotransferase, *TB* total bilirubin, *DB* direct bilirubin, *PLT* platelet count, *PT* prothrombin time, *INR* international normalized ratio
*P-value < 0.05

MVI-related radiomic signatures

MVI-related radiomic signatures based on the AP, PVP, DP and UP feature datasets were developed. After eliminating redundant features, 336, 384, 349 and 366 features were retained out of 1,584 features (396 features per phase) from the AP, PVP, DP and UP images. Furthermore, based on the seven, six, nine, and seven selected radiomics features screened by the LASSO algorithm, the corresponding radiomics signatures of the four phases were constructed. Table 2 summarizes the details of the selected features.

Performance of the different radiomics models

Twelve radiomics models were constructed by the LR, SVM, and Bayes modeling methods. The AP, PVP, DP, and UP radiomics signatures were used as the input factors for these radiomics models. The predictive performance of the different models in validation dataset is presented in table 3.

The AP radiomics signature achieved the higher AUC compared with the PVP, DP, and UP radiomics signatures in all modeling methods (table 3). Furthermore, the AP radiomics model established by LR demonstrated better estimation of the MVI risk,

with an AUC of 0.848 in the validation datasets, compared with the SVM model (AUC = 0.836) and Bayes model (AUC = 0.807). The DeLong test demonstrated a statistically significant difference between the AUCs of AP and DP by the LR method (P=0.033), and no significant difference were observed among the AUCs of radiomics model built using the LR, SVM and Bayes algorithms (P＞0.05) (figure 2).

Table 2. Selected features for the UP, AP, PVP and DP.

Feature parameter	OR (95% CI)
Unenhanced phase (N = 7)	
SizeZoneVariability	1.272(0.513-3.158)
Sphericity	0.421(0.225-0.786)
ShortRunHighGreyLevelEmphasis_angle90_offset1	0.954(0.453-2.009)
LongRunEmphasis_AllDirection_offset4_SD	1.163(0.520-2.599)
ShortRunEmphasis_AllDirection_offset4_SD	0.704(0.335-1.477)
GreyLevelNonuniformity_AllDirection_offset7_SD	2.201(0.287-16.848)
RunLengthNonuniformity_AllDirection_offset4_SD	3.048(0.467-19.874)
Arterial phase (N = 7)	
LowGreyLevelRunEm+B4:L12phasis_angle90_offset1	0.525(0.175-1.573)
HighGreyLevelRunEmphasis_AllDirection_offset7_SD	0.543(0.242-1.219)
Sphericity	0.365(0.190-0.703)
kurtosis	0.862(0.333-2.233)
Intensity Variability	1.658(0.732-3.755)
skewness	1.559(0.664-3.661)
ShortRunHighGreyLevelEmphasis_angle135_offset1	0.668(0.290-1.537)
Portal venous phase (N = 6)	
Compactness2	2.633(1.461-4.743)
ShortRunLowGreyLevelEmphasis_angle90_offset1	0.618(0.168-2.276)
ClusterProminence_angle90_offset7	1.245(0.638-2.428)
ShortRunEmphasis_AllDirection_offset4_SD	0.627(0.216-1.817)
ShortRunHighGreyLevelEmphasis_angle135_offset1	0.727(0.374-1.413)
RunLengthNonuniformity_angle90_offset4	2.587(1.017-6.577)
Delay phase (N = 9)	
GLCMEnergy_AllDirection_offset7	0.568(0.092-3.496)
SizeZoneVariability	2.184(0.954-5.001)
ZonePercentage	1.661(0.872-3.162)
ShortRunLowGreyLevelEmphasis_angle135_offset1	0.795(0.273-2.319)
Sphericity	0.249(0.112-0.554)
stdDeviation	0.477(0.175-1.297)
ClusterProminence_angle0_offset7	1.157(0.519-2.575)
InverseDifferenceMoment_angle45_offset7	0.724(0.245-2.143)
GLCMEnergy_angle45_offset4	0.841(0.234-3.015)

Seven, seven, six and nine features were ultimately selected in the UP, AP, PVP and DP by LASSO method, the P values of all features are less than 0.05.

Table 3. Predictive performance of three modeling methods in the validation dataset

Different models	Logistic Regression model				Support Vector Machine model				Bayes model			
	Accuracy	Sensitivity	Specificity	AUC	Accuracy	Sensitivity	Specificity	AUC	Accuracy	Sensitivity	Specificity	AUC
AP	0.789	0.643	0.875	0.848	0.737	0.643	0.792	0.836	0.789	0.643	0.875	0.807
PVP	0.737	0.571	0.833	0.818	0.816	0.786	0.833	0.815	0.658	0.429	0.792	0.768
DP	0.737	0.643	0.792	0.807	0.658	0.357	0.833	0.783	0.737	0.643	0.792	0.783
UP	0.737	0.571	0.833	0.783	0.737	0.429	0.917	0.756	0.711	0.429	0.875	0.757

AP arterial phase, PVP portal venous phase, DP delay phase, UP unenhanced phase, AUC area under the curve
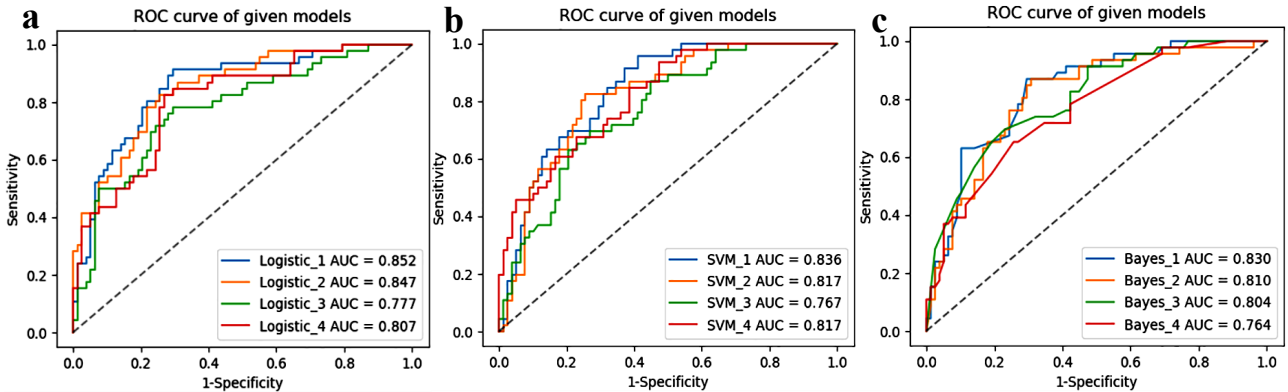

Figure 2. Comparison of receiver-operating characteristic (ROC) curves for the radiomics models derived from three modeling methods for the prediction of microvascular invasion. ROC curves of the logistic regression model **(a)**, support vector machine (SVM) model **(b)** and Bayes model **(c)** with the UP, AP, PVP and DP radiomics signatures as the input factors. _1 represents the AP signature, _2 represents the PVP signature, _3 represents the DP signature, and _4 represents the UP signature.

Clinical model construction

The LR method with better performance was selected from among the radiomics models, and the above four clinically factors were applied to construct the clinical prediction model. The AUCs were 0.776 in the training datasets and 0.807 in the validation datasets.

Performance of the combined model

The combined model integrating the effective clinical factors (MTD, AFP, PLT, and pathological grading) and the AP radiomics signature was established by LR method. The AUC, accuracy, sensitivity and specificity were 0.851, 82.6, 71.9 and 88.9% in the training datasets and 0.875, 84.2, 71.4 and 91.7% in the validation datasets respectively. In addition, the combined model showed better prediction performance than the other single radiomics and clinical models (table 4).

The calibration curve of this model yielded great consistency between the actual probabilities and predicted probabilities of MVI (figure 3). Moreover, the decision curve (figure 3) demonstrated that a net benefit can be obtained from our combined model.

MVI-predicting nomogram development and validation

A radiomics nomogram was built as a graphical presentation based on the combined model (figure 4). Adding the points of each risk factor results in the total number of points, which indicates the risk of MVI intuitively.

Table 4. Predictive performance of different models in Logistic Regression method

Different models	Training dataset(N=86)				Validation dataset(N=38)			
	Accuracy	Sensitivity	Specificity	AUC	Accuracy	Sensitivity	Specificity	AUC
AP	0.791	0.625	0.889	0.852	0.789	0.643	0.875	0.848
VP	0.767	0.625	0.852	0.849	0.737	0.571	0.833	0.818
DP	0.779	0.688	0.833	0.861	0.737	0.643	0.792	0.807
UP	0.756	0.531	0.889	0.821	0.737	0.571	0.833	0.783
CF	0.779	0.594	0.889	0.776	0.737	0.429	0.971	0.807
AP+CF	0.826	0.719	0.889	0.851	0.842	0.714	0.917	0.875

AP arterial phase, *PVP* portal venous phase, *DP* delay phase, *UP* unenhanced phase, *CF* clinical factor, *AUC* area under the curve
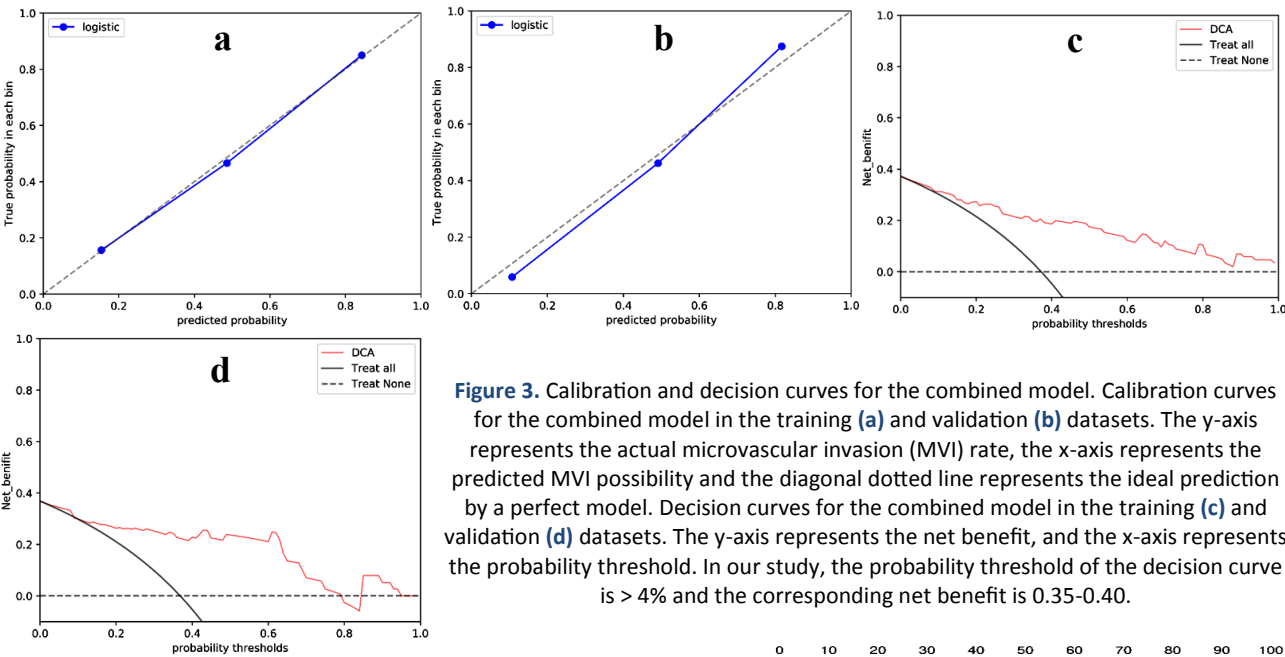

Figure 3. Calibration and decision curves for the combined model. Calibration curves for the combined model in the training **(a)** and validation **(b)** datasets. The y-axis represents the actual microvascular invasion (MVI) rate, the x-axis represents the predicted MVI possibility and the diagonal dotted line represents the ideal prediction by a perfect model. Decision curves for the combined model in the training **(c)** and validation **(d)** datasets. The y-axis represents the net benefit, and the x-axis represents the probability threshold. In our study, the probability threshold of the decision curve is > 4% and the corresponding net benefit is 0.35-0.40.

Figure 4. The nomogram obtained by combining the effective clinical factor (CF) and AP radiomics signature.

388

Int. J. Radiat. Res., Vol. 21 No. 3, July 2023
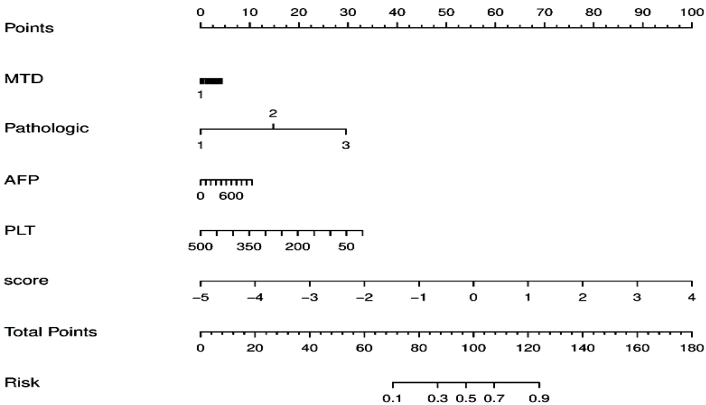
DISCUSSION

In this study, we developed and validated the machine learning model based on CT radiomic features that could effectively distinguish patients with or without MVI preoperatively. The AP radiomics signature exhibited higher accuracy and AUC values for preoperatively predicting MVI than the other phases. In addition, the LR model performed best in our study and the combined model that integrated effective CFs and the AP radiomics signature showed significant improvement compared with the radiomics signature or clinical model alone. Additionally, a nomogram based on the combined model provided a straightforward approach to demonstrate the individual risk for MVI in each patient with HCC.

Compared with traditional imaging characteristics, radiomics reflects potential and valuable micro-imaging features. Furthermore, the results are less affected by the subjective consciousness of radiologists [14]. Radiomics is swiftly evolving as a central imaging technology for personalized precision medicine in oncology [12, 17]. In our study, the radiomics model showed high accuracy for preoperatively predicting MVI.

Ma *et al.* [18] reported that the PVP radiomics model displayed better predictive performance than other phases. In contrast to this study, we demonstrated that the AP model based on radiomics signature performed better than the PVP, DP, and UP models. Our research results are based on a variety of modeling methods, and may be based on the following: (1) according to the hemodynamics, most of the small vessels entering the tumor mass are supplied by the hepatic artery, and obvious enhancement can be seen during the arterial phase of the enhanced scan [8, 19], (2) the obstruction of the minute portal venules by tiny tumor thrombus around the tumor may lead to a decrease or lack of venous blood supply, resulting in increased compensatory arterial perfusion [20, 21]. These characteristics can be well captured by feature extraction software in AP.

Our study discovered seven features [three histogram features (kurtosis, skewness, and IntensityVariability), three texture features (LGLRE, HGLRE, and SRHGLE) and one shape feature (sphericity)] closely related to the biological characteristics and heterogeneity of HCC in the AP radiomics model [22-24]. The histogram-based features were first-order statistics, which mainly relied on the intensity of the information statistics, reflecting the distribution of the gray values. To put it in practical terms, 'kurtosis' reflects the degree of gray contrast, where higher values indicate stronger heterogeneity, and 'skewness' represents the distribution of the pixel values. Texture features are second-order statistics that can be used to describe the complexity and distribution situation, the higher the value is, the more complicated the texture distribution. Because malignant tumors are more prone to invasion and degeneration, their heterogeneity is more apparent [22]. These radiomics features were identified in our study to be valuable for predicting MVI.

Former studies have used different single modeling methods to predict MVI before surgery. He *et al.* [16] constructed a radiomics model for MVI predictive, and the model exhibited average-to-good efficacy. Bakr *et al.* [15] also made a preliminary attempt to predict MVI. These studies have shown discrepancies in diagnostic performance. Our study further validated three commonly applied machine learning methods, and is a more comprehensive study of approaches for preoperatively predicting MVI. The accuracy, sensitivity, specificity and AUC value of the prediction model established by the LR algorithm in this study were slightly higher than those of the SVM and Bayes models. However, there was no statistically significant difference among the AUC values of the three modeling methods. LR is often preferred in the medical field due to its low computational cost, and it is easier to understand and implement than other algorithms [25]. SVM is suitable for small scale samples, significantly solving nonlinear and high-dimensional data, but it is challenging for solving multiclassification problems [26, 27]. Bayes is a supervised learning generative model with a stable classification efficiency. Its' main disadvantage is that it ignores interactions among the features, which may lead to feature redundancy [28]. The three modeling methods in our study have no obvious advantages in the preoperative prediction of HCC microvascular invasion, and it is difficult to reflect the characteristics of each modeling algorithm. Possibly due to the small sample size in this study and the unbalanced number of patients in the validation set.

Previous studies have noted a combined model's efficacy for cancer diagnosis and therapeutic effects [16, 29]. In our study, the combined radiomics-CF model showed superior predictive performance than either the CF model or the radiomics signature alone. This showed that a combination of different risk factors has a certain synergistic effect on the prediction of HCC MVI. Furthermore, the decision curve analysis implied that the combined model was clinically helpful, and may promote personalized therapy in HCC patients.

Our study inevitably has potential limitations that need to be addressed in future studies. First, some patient clinical indicators were missing due to incomplete preoperative examination items, and HCC patients without surgical treatment were excluded, which resulted in a small sample size and an uneven distribution in the MVI positive group. These factors ultimately lead to potential data selection bias and may influence the interpretation of the results.

Second, this study was conducted in a single-center, and a multi-institutional study should be performed to verify the results. Third, few cases had both CT and MR images in our study, so we did not include any MRI data. Additional studies are needed to determine whether MRI may lead to better results for predicting the histologic status in HCC based on the characteristics of multiple parameters. Finally, this study only selected three well-known modeling methods and did not comprehensively analyze all current modeling methods.

CONCLUSIONS

Radiomic parameters extracted from CT images show potential value to facilitate the prediction of MVI in HCC. A combined model that incorporated AP radiomics signatures and CFs achieved remarkable preoperative prediction of MVI. We compared different modeling methods for the preoperative diagnosis of MVI, which widened the choice of methods available to the reader. Future research should focus on reproducibility and robustness to explore standardization so that radiomics can be further developed into a useful, noninvasive tool in clinical practice.

REFERENCES

1. Sung H, Ferlay J, Siegel RL, Laversanne M, Soerjomataram I, Jemal A, Bray F (2021) Global Cancer Statistics 2020: GLOBOCAN Estimates of Incidence and Mortality Worldwide for 36 Cancers in 185 Countries. *CA Cancer J Clin,* **71:** 209-49.
2. Zhou M, Wang H, Zeng X, Yin P, Zhu J, Chen W, *et al.* (2019) Mortali-ty, morbidity, and risk factors in China and its provinces, 1990–2017: a systematic analysis for the Global Burden of Disease Study 2017. *Lancet,* **394:** 1145-58.
3. Ferlay J, Colombet M, Soerjomataram I, Mathers C, Parkin DM, Piñeros M, *et al.* (2019) Estimating the global cancer incidence and mortality in 2018: GLOBOCAN sources and methods. *International Journal of Cancer,* **144:** 1941-53.
4. Xie DY, Ren ZG, Zhou J, Fan J, Gao Q (2020) 2019 Chinese clinical guidelines for the management of hepatocellular carcinoma: updates and insights. *Hepatobiliary Surg Nutr,* **9:** 452- 63.
5. Vitale A, Trevisani F, Farinati F, Cillo U (2020) Treatment of hepatocellular carcinoma in the precision medicine era: From treatment stage migration to therapeutic hierarchy. *Hepatology,* **72:** 2206-18.
6. European Association for the Study of the Liver, European Organization for Research and Treatment of Cancer (2012) EASL–EORTC clinical practice guidelines: Management of hepatocellular carcinoma. *European Journal of Cancer,* **56:** 908- 43.
7. Kulik L and El-Serag HB (2019) Epidemiology and management of hepatocellular carcinoma. *Gastroenterology,* **156:** 477-91.e1.
8. Malloy PC (2019) Combination therapy in intermediate-stage hepatocellular carcinoma: Do we need to know about microvascular invasion? *Radiology,* **292:** 248-9.
9. Zheng J, Seier K, Gonen M, Balachandran VP, Kingham TP, D'Angelica MI, *et al.* (2017) Utility of Serum Inflammatory Markers for Predicting Microvascular Invasion and Survival for Patients with Hepatocellular Carcinoma. *Ann Surg Oncol,* **24:** 3706-14.
10. Zhang XP, Wang K, Wei XB, Li LQ, Sun HC, Wen TF, *et al.* (2019) An Eastern hepatobiliary surgery hospital microvascular invasion scoring system in predicting prognosis of patients with hepatocellular carcinoma and microvascular invasion after R0 liver resection: A large-scale, multicenter study. *Oncologist,* **24:** e1476-88.
11. Wei Y, Huang Z, Tang H, Deng L, Yuan Y, Li J, *et al.* (2019) IVIM improves preoperative assessment of microvascular invasion in HCC. *European Radiology,* **29:** 5403-14.
12. Lambin P, Leijenaar RTH, Deist TM, Peerlings J, de Jong EEC, van Timmeren J, *et al.* (2017) Radiomics: the bridge between medical imaging and personalized medicine. *Nat Rev Clin Oncol,* **14:** 749-62.
13. Gillies RJ, Kinahan PE, Hricak H (2016) Radiomics: Images are more than pictures; They are data. *Radiology,* **278**: 563-77.
14. Liu Z, Wang S, Dong D, Wei J, Fang C, Zhou X, *et al.* (2019) The Applications of radiomics in precision diagnosis and treatment of oncology: Opportunities and challenges. *Theranostics,* **9:** 1303-22.
15. Bakr S, Echegaray S, Shah R, Kamaya A, Louie J, Napel S, *et al.* (2017) Noninvasive radiomics signature based on quantitative analysis of computed tomography images as a surrogate for microvascular invasion in hepatocellular carcinoma: a pilot study. *J Med Imaging,* **4:** 041303.
16. He M, Zhang P, Ma X, He B, Fang C, Jia F (2020) Radiomic feature-based predictive model for microvascular invasion in patients with hepatocellular carcinoma. *Front Oncol,* **10:** 574228.
17. Verma V, Simone CB 2nd, Krishnan S, Lin SH, Yang J, Hahn SM (2017) The rise of radiomics and implications for oncologic management. *J Natl Cancer Inst,* **109:** page numbers??
18. Ma X, Wei J, Gu D, Zhu Y, Feng B, Liang M, Wang S, Zhao X, Tian J (2019) Preoperative radiomics nomogram for microvascular invasion prediction in hepatocellular carcinoma using contrast-enhanced CT. *Eur Radiol,* **29:** 3595-3605.
19. Feng ST, Jia Y, Liao B, Huang B, Zhou Q, Li X, *et al.* (2019) Preoperative prediction of microvascular invasion in hepatocellular cancer: a radiomics model using Gd-EOB-DTPA-enhanced MRI. *Eur Radiol,* **29:** 4648-59.
20. Choi JY, Lee JM, Sirlin CB (2014) CT and MR imaging diagnosis and staging of hepatocellular carcinoma: part II. Extracellular agents, hepatobiliary agents, and ancillary imaging features. *Radiology,* **273:** 30-50.
21. Thompson SM, Wells ML, Andrews JC, Ehman EC, Menias CO, Hallemeier CL, *et al.* (2018) Venous invasion by hepatic tumors: imaging appearance and implications for management. *Abdom Radiol,* **43:** 1947-67.
22. El-Sayes N, Vito A, Mossman K (2021) Tumor heterogeneity: A great barrier in the age of cancer immunotherapy. *Cancers,* **13:** 806.
23. Grossmann P, Stringfield O, El-Hachem N, Bui MM, Rios Velazquez E, Parmar C, *et al.* (2017) Defining the biological basis of radiomic phenotypes in lung cancer. *Elife,* **6:** e23421.
24. Mokrane FZ, Lu L, Vavasseur A, Otal P, Peron JM, Luk L, *et al.* (2020) Radiomics machine-learning signature for diagnosis of

hepatocellular carcinoma in cirrhotic patients with indeterminate liver nodules. *Eur Radiol, 30:* 558-70.

25. Stylianou N, Akbarov A, Kontopantelis E, Buchan I, Dunn KW (2015) Mortality risk prediction in burn injury: Comparison of logistic regression with machine learning approaches. *Burns, 41:* 925-34.

26. Zou ZM, Chang DH, Liu H, Xiao YD (2021) Current updates in machine learning in the prediction of therapeutic outcome of hepatocellular carcinoma: what should we know? *Insights Imaging, 12:* 31.

27. Beunza JJ, Puertas E, García-Ovejero E, Villalba G, Condes E, Koleva G, *et al.* (2019) Comparison of machine learning algorithms for clinical event prediction (risk of coronary heart disease). *J Biomed Inform, 97:* 103257.

28. Uddin S, Khan A, Hossain ME, Moni MA (2019) Comparing different supervised machine learning algorithms for disease prediction. *BMC Med Inform Decis Mak, 19:* 281.

29. Xu Y, Li R, Li X, Dong N, Wu D, Hou L, Yin K, Zhao C (2020) An autophagy-related gene signature associated with clinical prognosis and immune microenvironment in gliomas. *Front Oncol, 10:* 571189.